ORIGINAL RESEARCH ARTICLE

Analysis of influence of ripple parameters of heat storage elements on flow and heat transfer performance

Yuzhen Yu, Haikuan Di*, Bo Zhao, Haiying Li

School of Mechanical Engineering North China University of Technology, Tangshan 063210, China. E-mail: dihaikuan_1996@163.com

ABSTRACT

In order to study the influence of the corrugated angle and width of enamel heat storage element on the flow and heat transfer performance, a certain enamel heat storage element was numerically simulated by FLUENT software, and the variation curves of internal flow field velocity, temperature distribution, Nusselt number and drag coefficient with Reynolds number were obtained when the corrugated angle and width of the heat storage element were different. The simulation results show that when the ripple inclination increases from 20° to 60°, the resistance coefficient of the heat storage element increases, and the Nusselt number increases, and the increase of the resistance coefficient is greater than that of the Nusselt number; when the ripple width increases from 6 mm to 10 mm, the increase of resistance coefficient is small, and the increase of Nusselt number is large.

Keywords: Rotary Air Preheater; Heat Storage Element; Resistance Coefficient; Nusselt Number

1. Introduction

Rotary air preheater is a kind of heat exchange device, which is widely used in thermal power plants. Its core component is the heat storage elements arranged in the rotor. The flow and heat transfer characteristics of the heat storage elements determine whether the rotary air preheater can operate safely and efficiently[1,2]. Therefore, studying the heat transfer and resistance characteristics of heat storage elements and the distribution of internal temperature field under different structural parameters is of great significance to improve the flow and heat transfer performance of rotary air preheater and ensure the safe and efficient operation of boiler. Scholars at home and abroad have studied the flow and heat transfer performance of heat storage elements. Wang[3] found that controlling the frictional resistance along the way is the key to reducing the flow resistance of heat storage elements through a large-scale hot air tunnel experimental system. Chi[4] proposed a scheme to measure the temperature of the low-temperature heating surface of the rotary air preheater. Mohammed[5] found that the effect of convective heat transfer can be enhanced by adding ripple to the heat storage element. Focke[6] found that when the corrugation angle is large, the increase of the corrugation angle is small, and the increase of the convection heat transfer coefficient is small. Yang[7] conducted enamel transformation on the heat storage element and found that the comprehensive convective heat transfer performance was significantly improved.

This paper studies the heat storage elements with different corrugated structure parameters by numerical simulation, analyzes the temperature and velocity distribution of the internal flow field, and obtains the influence of the corrugated inclination and width on the flow and heat transfer performance of the heat storage elements.

2. Numerical simulation

2.1 Rotary air preheater

Rotary air preheater is mainly composed of rotor, heat transfer element, shell, beam, sector plate and sealing device[8]. The boiler flue gas flows in through the flue gas channel from top to bottom, and the air flows out of the primary air and secondary air outlets from bottom to top. Each revolution of the rotor, the heat storage element absorbs and releases heat once[9,10]. There are two 30° transition zones in the rotor, in which neither flue gas nor air passes through, which plays the role of separating flue gas and air. The structure is shown in **Figure 1**.
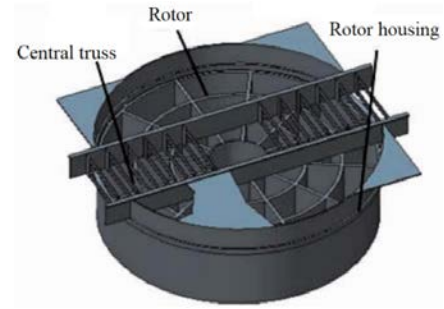

Figure 1. Structure of rotary air preheater.

2.2 Simulation objects and model assumptions

2.2.1 Simulation object

The simulation object is an enamel heat storage element, the structure is shown in **Figure 2**, and the structural parameters are shown in **Table 1**.
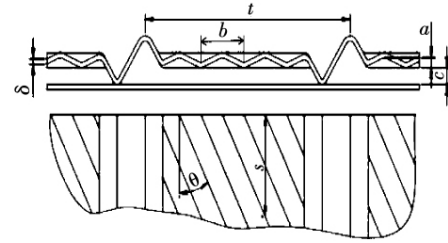

Figure 2. Structure of enamel heat storage element.

Table 1. Structural parameters of heat storage elements

Plate thickness δ/mm	Equivalent diameter d/mm	Span t/mm	Ripple gap c/mm	Surface density/m⁻¹	Corrugated plate corrugated wave height a/mm	Ripple width of corrugated plate b/mm
1.15	12.54	65.9	5.3	398.8	3.03	8

Table 2. Structural parameters for different inclination of corrugation

Corrugation inclination θ/(°)	Equivalent diameter D/mm	Ripple axial pitch s/mm
20	12.48	8.62
30	12.54	9.35
40	12.60	10.51
50	12.64	12.6
60	12.75	16.2
70	12.27	23.68

Table 3. Structural parameters for different ripple width

Ripple width b/mm	Equivalent diameter D/mm	Ripple axial pitch s/mm
6	12.27	12.1
7	12.53	14.3
8	12.75	16.2
9	12.9	18.1
10	13	20.4

Under the condition that the ripple width and height of the heat storage element remain unchanged, change the ripple inclination angle to 20°, 30°, 40°, 50°, 60° and 70° in turn, and the changed structural parameters are shown in **Table 2**.

When the corrugation angle of the heat storage

55

element is 60° and the height remains unchanged, the corrugation width is changed to 6, 7, 8, 9 and 10 mm in turn. The changed structural parameters are shown in **Table 3**.

When changing the ripple parameters, the equivalent diameter of the heat storage channel will change, and the calculation formula[11] is:

$$D = \frac{4A}{L}$$

(1)

Where: A—sectional area of flow channel between corrugated plate and flat plate of heat storage element, mm^2; L—wet perimeter of flow channel between corrugated plate and flat plate of heat storage element, mm.

2.2.2 Model assumptions and simplification

For the convenience of numerical simulation, the following assumptions and simplifications are made:

Because the internal structure of the heat storage element is complex, and the waveform changes periodically. Therefore, a flow unit of heat storage element is taken as the research object[12]; the wall thickness of heat storage element is 0[13]; air is regarded as compressible Newtonian fluid; the heat storage element is simplified into a constant wall temperature model; the length of the heat storage element is 500 mm (the inlet effect can be ignored)[14].

2.3 Physical model and boundary conditions

2.3.1 Physical model and grid division

The required model is established in CREO software, tetrahedral mesh division is adopted for all plate heat storage elements, and an expansion layer is set near the wall to solve the high gradient flow change and complex physical characteristics near the wall. When the inclination is 20°, the number of grid units is 1.1962 million, when the inclination is 50°, the number of grid units is 1.097 million, and when the inclination is 70°, the number of grid units is 1.054 million, which has passed the verification of grid independence. The grid division is shown in **Figure 3**.
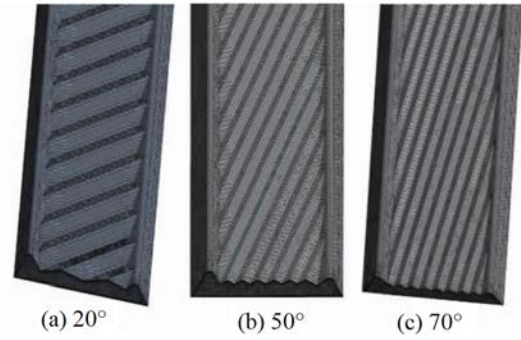

(a) 20° (b) 50° (c) 70°

Figure 3. Grid division.

2.3.2 Boundary conditions and model settings

Fluent software is used for three-dimensional numerical simulation, using mass conservation equation, momentum conservation equation, and slip free boundary conditions. The inlet temperature is 293 K, the wall temperature is 373 K, and air is used as the flowing medium (density ρ 1.225 kg/m^3, dynamic viscosity μ is 1.75 × 10^{-5} Pa·s, thermal conductivity λ is 0.0242 W/(m·K)), and other parameter settings are shown in **Table 4**.

Table 4. Parameter settings

Parameter	Settings
Viscous model	k-ε Model
Near wall treatment	Enhanced wall treatment
Pressure velocity coupling	Simple format
Discretization of momentum equation and energy equation	Quick format
Wall thermal boundary condition	Constant temperature
Inlet boundary conditions	Speed inlet
Exit boundary conditions	Free outflow

2.3.3 Evaluation method

The flow and heat transfer performance of the regenerative element of the rotary air preheater mainly depends on the resistance coefficient and convection heat transfer coefficient between the medium and the regenerative plate[15]. The greater the resistance coefficient is, the worse the flow performance of the heat storage element will be. The convective heat transfer coefficient of the heat storage element refers to the heat transfer capacity between the air and the surface of the heat storage element. The higher the value, the better the heat transfer performance of the heat storage element. Further, the variation law of Nusselt number Nu with Reynolds number Re can be used to indi-

cate the intensity of convective heat transfer of the heat storage element[16,17]. The resistance coefficient[18] is:

$$f = \frac{2d\Delta p}{l\rho v^2}$$

(2)

Where: Δp—frictional resistance of air flowing through the heat storage element, Pa; ρ—air density, kg/m³; v—actual flow speed of air flowing through the element, m/s; d—equivalent diameter of heat storage element, m; l—length of heat storage element, m.

The Nusselt number formula[19] is:

$$Nu = \frac{ad_{dl}}{\lambda}$$

(3)

Where: a—Convective heat transfer coefficient, W/(m²·K); d_{dl}—equivalent diameter of heat storage element, m; λ—Thermal conductivity of fluid medium, W/(m·K).

Reynolds number is calculated as:

$$Re = \frac{\rho v d}{\mu}$$

(4)

Where: v—actual flow speed of air flowing through the flow channel of the element, m/s; μ—Dynamic viscosity of air, Pa·s.

3. Results and analysis

3.1 Influence of corrugation angle

3.1.1 Velocity nephogram

When the inlet wind speed is 10 m/s, the outlet velocity nephogram of the heat storage element with the wavy inclination of 20°, 30°, 40°, 50°, 60° and 70° is shown in **Figure 4**.

It can be seen from **Figure 4** that the maximum speed at the outlet of the heat storage channel is the maximum when the ripple angle is 20°, and the value is 31.118 m/s. The maximum speed at the outlet of the heat storage channel with the ripple angle of 70° is the minimum, and the value is 17.539 m/s. According to the report function in **Figure 4** in fluent software, the average speed at the outlet of 20°−70° heat storage channel is 10.48, 10.09, 10.05, 9.91, 9.87 and 9.99 m/s respectively.
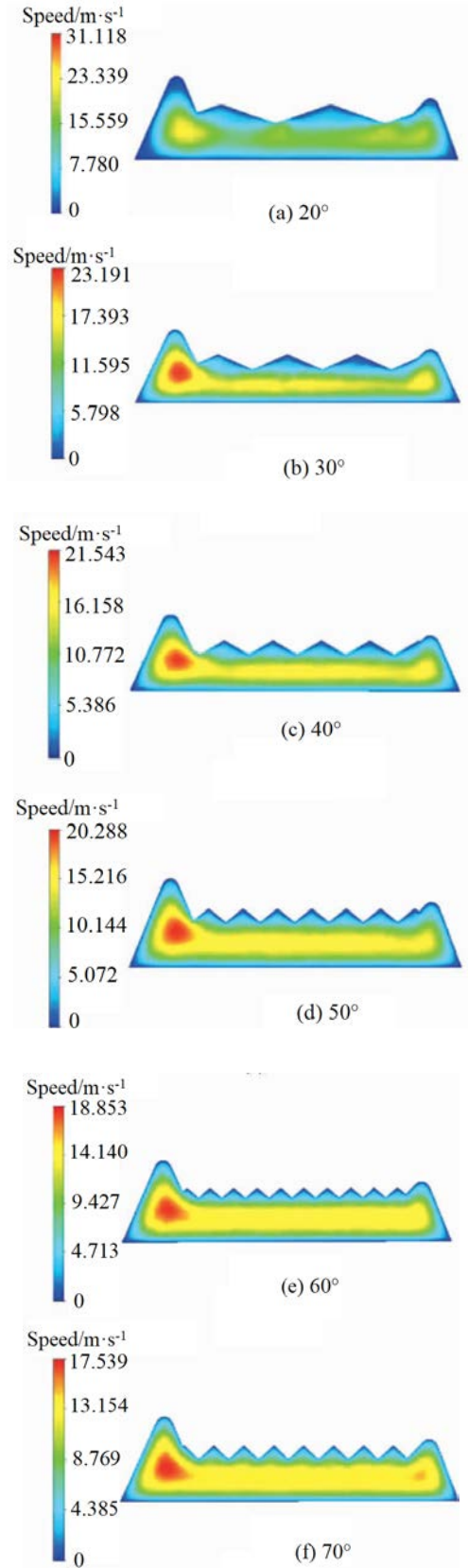

Figure 4. Contour of outlet velocity of thermal storage element.

When the ripple angle increases from 20° to 60°, the average speed at the outlet of heat storage channel decreases in turn. With the increase of cor-

rugation angle, the number of oblique corrugations decreases, the resistance of heat storage channel to air decreases, and the speed gradually decreases. The corrugated channel of the 70° corrugated heat storage element is narrow and close to vertical, and part of the air flows directly from the channel, so the speed increases.

3.1.2 Temperature nephogram

When the inlet wind speed is 10 m/s, the temperature nephogram at the inlet of the heat storage channel with different corrugated inclination is shown in **Figure 5**.

Using the report function in **Figure 5** in fluent software, the average temperature at the 16 mm section at the inlet of the heat storage element with a ripple inclination of 20°−70° is 318.84, 319.90, 320.75, 321.68, 323.58 and 320.10 K respectively. The heat exchange performance of the heat storage element is the best when the ripple angle is 60°, and the worst when the ripple angle is 20°. When the wavy angle is 20°, the disturbance in the direction of temperature gradient is very small, and there is not enough convective heat transfer between the air and the wall. When the corrugated angle is 60°, the contact area between the air and the heat storage element is the largest, which is conducive to enhancing convective heat transfer.
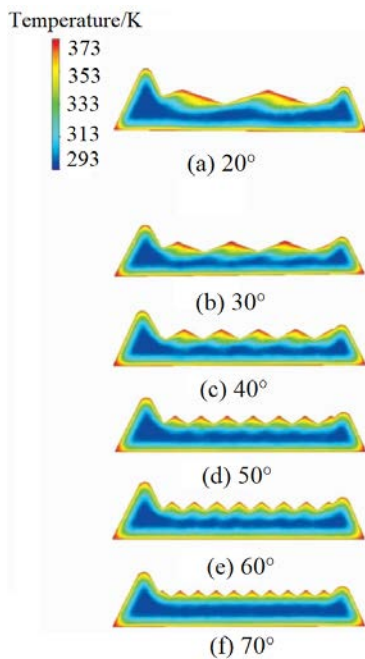

Figure 5. Temperature contour at 16 mm from the inlet of thermal storage element.

3.2 Influence of ripple width

3.2.1 Velocity nephogram

When the inlet wind speed is 10 m/s, the ripple angle is 60°, and the outlet velocity nephogram of the heat storage channel when the ripple width is 6, 7, 8, 9 and 10 mm is shown in **Figure 6** respectively.

It can be seen from **Figure 6** that with the increase of ripple width, the outlet velocity of the heat storage channel increases. When the ripple width is 6−10 mm, the average velocity of the outlet section of the heat storage channel is 9.48, 9.64, 9.87, 9.98 and 10.01 m/s respectively.
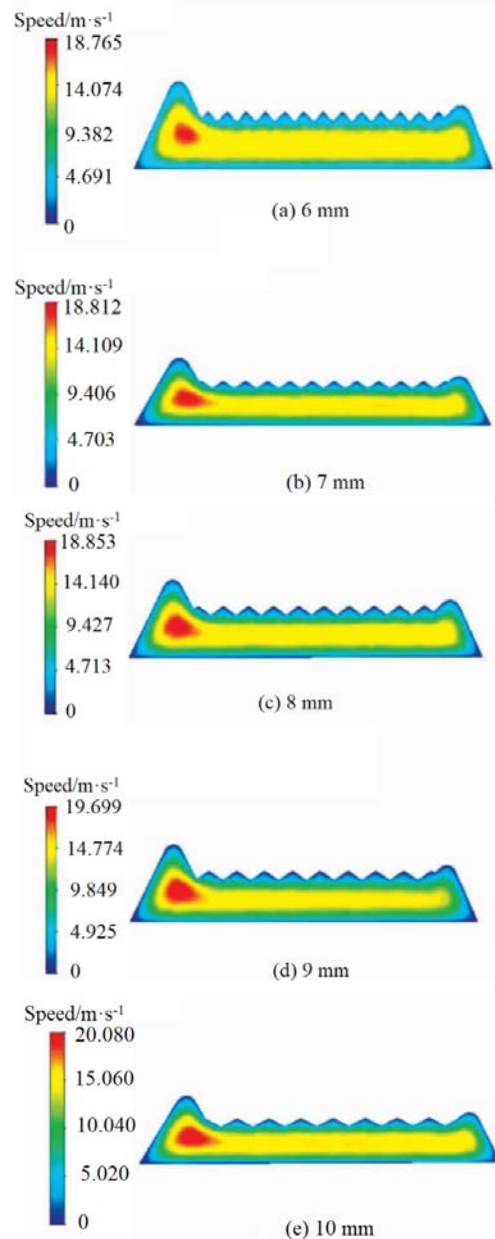

Figure 6. Contour of lateral velocity at the outlet of thermal storage element.

When the ripple width is 10 mm, the outlet speed of the heat storage channel is the highest, because the heat transfer effect is good, the air volume expands more, and the cross-sectional flow rate increases. According to the field synergy theory[20], compared with other ripple widths, the velocity field and temperature gradient field of the 10 mm width heat storage element have better coherence and stronger convective heat transfer performance.

3.2.2 Temperature nephogram

When the inlet wind speed is 10 m/s, the corrugated angle is 60°, and the corrugated width of the heat storage element is 6, 7, 8, 9 and 10 mm, the 14 mm temperature cloud diagram at the inlet of the heat storage channel is shown in **Figure 7**.
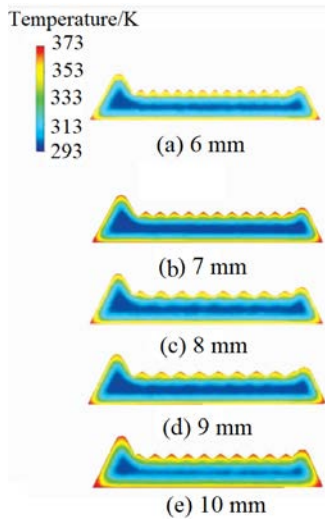

Figure 7. Temperature contour at 14 mm of the inlet of thermal storage element.

In fluent software, using the report function in **Figure 7**, the average temperature at the 14 mm section at the inlet of the heat storage channel with a ripple width of 6, 7, 8, 9 and 10 mm is 316.80, 318.78, 319.00, 319.44 and 319.75 K respectively. When the ripple width is 10 mm, the heat exchange performance of the heat storage element is the best, and the heat exchange performance of the 6 mm heat storage element is the worst. Increasing the ripple width can increase the contact area between air and heat storage elements, which is conducive to enhancing convective heat transfer.

4. Heat transfer and flow characteristics

4.1 Influence of corrugation angle on heat transfer coefficient and resistance coefficient

Numerical simulation is carried out by changing the inlet velocity of the heat storage element with a corrugated inclination of 20°–70°. Then use the report function in fluent software to obtain the parameters such as pressure loss and convective heat transfer coefficient of all heat storage elements.

The variation of resistance coefficient of heat storage elements with different corrugated inclination with Reynolds number is shown in **Figure 8**. It can be seen from **Figure 8** that the resistance coefficient of heat storage elements with different corrugated angles decreases with the increase of Reynolds number. When the corrugated angle is 20°–60°, the resistance coefficient of heat storage elements increases with the increase of the degree of corrugated angle, of which 40° and 50° increase relatively more. The drag coefficient decreases when the ripple angle is 70° compared with 60°, less at low Reynolds number and more at high Reynolds number. When the corrugated angle is 70°, the internal structure of the heat storage channel is not easy to cause air vortex, and the local pressure loss is small. Therefore, the resistance coefficient is reduced. The flow performance of the heat storage element is the best when the ripple angle is 20° and the worst when it is 60°. Comparing **Figure 8** with moody figure, the results are consistent, which proves that the results are reliable.
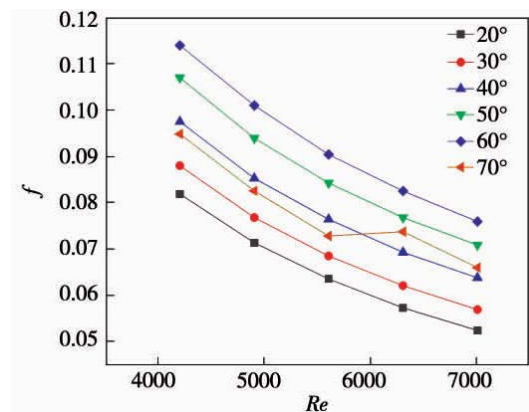

Figure 8. Relationship between resistance coefficient and corrugation angle.

The variation of Nusselt number with Reynolds number of heat storage elements with different corrugated inclination is shown in **Figure 9**. It

can be seen from **Figure 9** that the Nusselt number of heat storage elements with different corrugated inclination increases with the increase of Reynolds number. When the corrugated inclination is 20°–60°, with the increase of the degree of corrugated inclination, the Nusselt number of heat storage elements increases and the convective heat transfer performance improves. Taking the working condition of inlet speed of 10 m/s as an example, compared with 20°, the Nusselt number of 30°–70° corrugated heat storage elements increases by 1.22%, 5.01%, 8.62%, 12.37% and 2.33% respectively. When the corrugated angle is 70°, part of the air flows directly from the heat storage channel, with less heat exchange, so the Nusselt number increases less. The heat transfer performance is the best when the wavy angle is 60°. The wavy angle is more conducive to the disturbance of the air, making the boundary layer smaller and the heat transfer more sufficient.
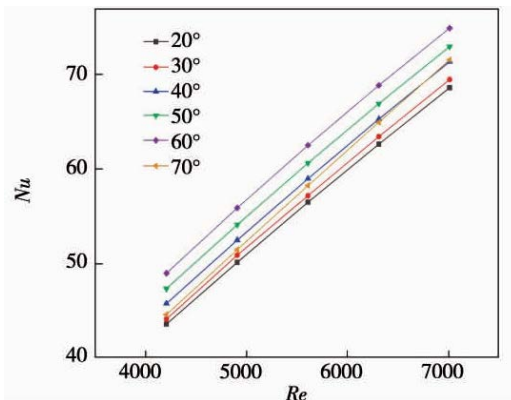

Figure 9. Relationship between Nusselt number and corrugation angle.

4.2 Effect of ripple width on heat transfer coefficient and resistance coefficient

Change the inlet velocity of heat storage elements with different ripple widths, and conduct numerical simulation respectively. The change of resistance coefficient of heat storage elements with different ripple widths with Reynolds number is shown in **Figure 10**. It can be seen from **Figure 10** that the resistance coefficient of the heat storage element increases with the increase of the ripple width. Taking the inlet speed of 10 m/s as an example, compared with the ripple width of 6 mm, the resistance coefficient of 10 mm heat storage element increases by only 0.83%, indicating that the

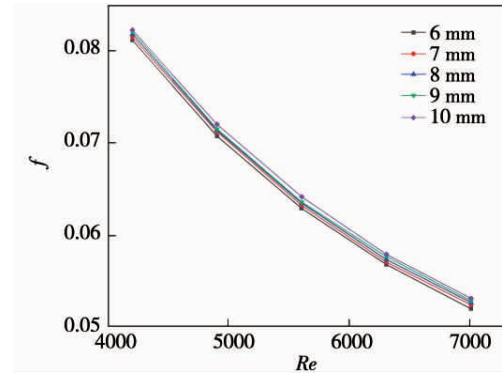ripple width has little effect on the flow resistance of heat storage element.

Figure 10. Relationship between resistance coefficient and ripple width.

The relationship between Nusselt number and Reynolds number of heat storage elements with different ripple widths is shown in **Figure 11**. It can be seen from **Figure 11** that with the increase of ripple width, the Nusselt number of heat storage elements increases, especially when it increases from 6 mm to 7 mm, an increase of 23.9%.
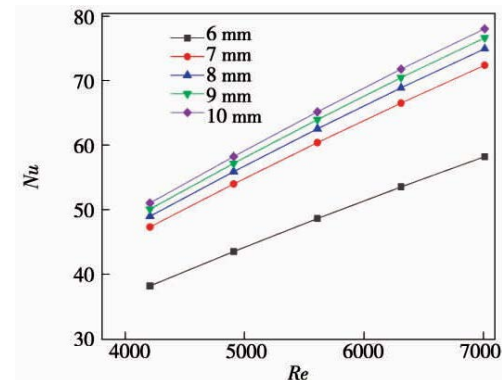

Figure 11. Relationship between Nusselt number and ripple width.

4.3 Numerical simulation reliability verification

In order to verify the reliability of the numerical simulation, the simulation results are compared with the simulation experimental results in literature[12]. When the ripple angle increases from 15° to 60°, the resistance coefficient increases and the Nusselt number increases. The simulation results are basically consistent with this paper, indicating that the conclusion is reliable.

5. Conclusion

(1) When the corrugation angle increases from

20° to 60°, the resistance coefficient increases, the Nusselt number increases, and the heat transfer performance of the heat storage element improves. When the inlet speed is 6 m/s, compared with the ripple inclination of 60°, the resistance coefficient of 70° is reduced by 11.3%, and the Nusselt number is reduced by 9.81%.

(2) When the ripple angle is 60°, when the ripple width of the heat storage element increases from 6 mm to 10 mm, the resistance coefficient increases and the Nusselt number increases, and the increase of Nusselt number is much higher than that of the resistance coefficient.

(3) Both the corrugation angle and the corrugation width are important factors affecting the Nusselt number of heat storage elements. Compared with the corrugation width, the corrugation angle has a greater impact on the resistance coefficient.

Acknowledgement

Conflict of interest

The authors declared no conflict of interest.

References

1. Shu S. Huizhuanshi kongqi yureqi huanre yuanjian shouming yingxiang yinsu (Chinese) [Factors affecting the life of heat exchange elements of rotary air preheater]. Science and Technology Innovation and Application 2019; (19): 74–76.
2. Wang Y, Chen G, Wang Z, *et al.* A review on seal technology of rotary air preheaters. Thermal Power Generation 2015; 44(8): 1–7.
3. Wang Q, Wang E, Mao M. Experimental research on friction characteristics of heat transfer elements of rotary air preheater. Boiler Technology 2011; 42(6): 10–12.
4. Chi Z, Pan W. Experimental studies on measuring the cold end metal temperature of 600mw rotating air heater. Proceedings of the CSEE 2002; 22(11): 129–131.
5. Mohammed HA. The effect of geometrical parameters of a corrugated channel with in out-of-phase arrangement. International Communications in Heat and Mass Transfer 2012; 19 (23): 1044–1051.
6. Focke WW, Zachariades J. The effect of the corrugation inclination angle on the thermohydraulic performances of the heat exchangers. Hear Mass Transfer 1985; 28(8): 1469–1479.
7. Yang X, Gao J, Wei R. Experimental study on heat transfer and fluid flow characteristics of cold and elements in air preheater before and after enamel retrofit. Boiler Technology 2016; 47(1): 22–25.
8. Cai M. Comparison of different manners for air preheater leakage control. Boiler Technology 2011; 42(2): 8–13.
9. Wang H, Bi X, Si F, *et al.* Comprehensive air leakage distribution models for rotary air preheaters of 300 MW units. East China Electric Power 2006; 34(1): 44–48.
10. Chen X, Wang L, Yang Y. Influence of flow arrangement pattern on thermal performance of tri-sector rotary regenerative air preheater and deposition rule for ammonium bisulfate. Journal of Engineering for Thermal Energy and Power 2019; 34(8): 102–108.
11. Wang J. Calculation of equivalent diameter in the pipeline. Journal of Liaoning University of Petroleum and Chemical Technology 2005; 25(3): 69–70.
12. Gao J, Zhang L, Wei R, *et al.* Analysis of influence of structure parameters of enamel heat storage elements on their heat transfer and flow characteristics. Journal of North China Electric Power University 2016; 43(3): 76–80.
13. Wei R, Yang X, Gao J, *et al.* Three-dimensional numerical study on the heat transfer and fluid flow of the heat transfer elements of rotary air preheater. Journal of North China Electric Power University 2015; 42(1): 58–62.
14. Qu Z. Numerical simulation of rotary air preheater [PhD thesis]. Beijing: North China Electric Power University; 2014.
15. Zhang Q, Jin X, Wang E, *et al.* Experimental research on thermal performance of heat transfer elements in rotary air preheater. Boiler Technology 2011; 42(3): 6–8.
16. Zhan H, Zhang X, Li Y, *et al.* Fundamentals of engineering heat transfer. Beijing: Sinopec Press; 2014.
17. Zhang L, Nie P, Liu W, *et al.* Single-blow transient test on the thermal-hydraulic performance of the composite corrugated plate. Proceedings of the CSEE 2017; 37(22): 6675–6680.
18. Mao M, Wang E, Wang Q. Experimental research on friction characteristics of the heat transfer elements of rotary air preheater. Boiler Technology 2012; 43(4): 13–15.
19. Gu X. Numerical simulation and experimental study on heat transfer and flow of enamel heat storage element of rotary air preheater [MSc thesis]. Beijing: North China Electric Power University; 2015.
20. Nolan M. Molecular adsorption on the doped (110) ceria surface. Journal of Physical Chemistry C 2009; 113(6): 2425–2432.